Hindawi
Journal of Nanomaterials
Volume 2022, Article ID 5938952, 13 pages
https://doi.org/10.1155/2022/5938952

Research Article

One-Put Ferula-Mediated Synthesis of Biogenic Silver Nanoparticles with More Antimicrobial Effect and Promising Human Cell Biocompatibility

Ahmad Gholami,[1,2,3] **Seyyed Mojtaba Mousavi**,[4] **Ali Shomali**,[2] **Seyyed Alireza Hashemi**,[5] **Seyedeh Narjes Abootalebi**,[1,6] **Wei-Hung Chiang**,[4] **Alireza Barzegar**,[7] **Mansooreh Shokripoor**,[8] **and Abdolali Mohaghegh Zadeh**[3,7]

[1]*Biotechnology Research Center, Shiraz University of Medical Sciences, Shiraz, Iran*
[2]*Department of Pharmaceutical Biotechnology, School of Pharmacy, Shiraz University of Medical Sciences, Shiraz, Iran*
[3]*Pharmaceutical Sciences Research Center, Shiraz University of Medical Sciences, Shiraz, Iran*
[4]*Department of Chemical Engineering, National Taiwan University of Science and Technology, Taiwan*
[5]*Nanomaterials and Polymer Nanocomposites Laboratory, School of Engineering, University of British Columbia, Kelowna, BC, Canada*
[6]*Department of Pediatrics, School of Medicine, Shiraz University of Medical Sciences, Shiraz, Iran*
[7]*Department of Pharmacognosy, School of Pharmacy, Shiraz University of Medical Sciences, Shiraz, Iran*
[8]*Department of Pathology, School of Medicine, Shiraz University of Medical Sciences, Shiraz, Iran*

Correspondence should be addressed to Abdolali Mohaghegh Zadeh; mohaghegh@sums.ac.ir

Received 6 January 2022; Revised 1 August 2022; Accepted 10 August 2022; Published 15 September 2022

Academic Editor: Carmen Lizette Del Toro S nchez

The biogenic synthesis of silver nanoparticles has recently attracted more attention to counter microbial resistance, which has been one of the medical concerns in the last decade. This research expresses the biogenic synthesis of silver nanoparticles utilizing Ferula assafoetida aqueous extract (Fer@AgNP) as a reducing and capping agent. The total parts of the plant were extracted from an aqueous solution (FerEX) and characterized using GC/MS apparatus. The Fer@AgNP and chemically synthesized silver nanoparticles (AgNPs) were characterized using UV-vis, Fourier transform infrared (FTIR) spectroscopies, field emission-scanning transmission electron microscopy, powder X-ray diffraction analysis, and energy-dispersive X-ray spectroscopy. The impacts of nanoparticles and FerEX were evaluated against four pathogenic bacterial strains, including Staphylococcus aureus, Escherichia coli, Salmonella typhi, and Enterococcus faecalis, using the microdilution method. The biocompatibility of compounds was also evaluated on human cell line L-929 using MTT and human blood cells using the hemolytic assay. The major compounds found in FerEX were sulfur-containing compounds such as butyl disulfides (45.36%) and monoterpenes such as α-pinene (25.66%), β-pinene (16.31%), and ocimene (7.26%). The characterizations of materials confirmed the hexagonal structure of AgNPs. The sizes of cAgNP and Fer@AgNP were about 42.7 nm and 22.5 nm. The antimicrobial activity of Fer@AgNP was considerably developed and reached MIC values ranging from 10 to 50 μg/mL compared to AgNP, which showed MIC values ranging from 50 to 100 μg/mL. The biocompatibility assessment showed that the Fer@AgNP was improved compared to AgNP and had a minimal toxic impact on the normal fibroblast cell line. The Fer@AgNP also indicated outstanding compatibility with human RBCs. The results illustrated that biosynthesized Fer@AgNPs have improved antimicrobial efficacy against Gram-negative and Gram-positive pathogenic bacteria with promising biocompatibility and can be used as potential antibacterial agents.

1. Introduction

Universal health problems associated with environmental concerns have led to a focus on the technology of green chemistry as an environmentally friendly process [1]. The development of antibiotic-resistant pathogens, which caused the increasing use of antibiotics, is one of the recent global health problems [2]. Therefore, efforts are being made to look for new alternatives to stop antibiotic-resistant microorganisms' development. Silver nanoparticles (AgNPs) have primarily been used against different microbial pathogens and exhibited a promising way of resolving the microbial crisis [3]. Although various methods have been developed to convert silver ions to AgNP chemically, they are most costly and time-consuming, involve high pressure and temperature, and have a negative environmental influence since hazardous chemicals are included in such conversions [4]. Biogenic synthesis of nanoparticles using natural products showed an advantage over other methods since it is simple and cost-effective and produces a stable product [5]. Biogenic synthesis is also considered more valuable than different approaches in some aspects due to more profitable delivered NPs, higher solidness, and their nontoxicity [6, 7].

In the last decade, the biogenic synthesis of AgNP has attracted extensive attention with the aid of plant extract as a reducing and capping agent [7]. Because of their availability, tolerability, biocompatibility, and lower cost than chemical reagents, plant extracts are preferred for the biogenic synthesis of nanomaterials. Since plant extracts contain several biologically active-secondary metabolites such as terpenoids, phenolic compounds, alkaloids, flavonoids, and glucosinolates, the resulting biogenic nanomaterials may show improved properties in terms of biological effects such as antimicrobial effects [8].

Various plant extracts' antimicrobial and cytotoxic activity has been considered in the last decades [9–11]. The *Ferula* species (Apiaceae) comprises around 170 species worldwide, of which thirty species are found in South and Southwest Asia. The properties of *Ferula assafoetida*, widely used in traditional medicine as an antimicrobial treatment, have been investigated in recent years. It has fascinating biological activities, from antiproliferative to anti-inflammatory to neuroprotective [12]. There are also some reports on the pharmacological effects of *Ferula assafoetida*, such as antibacterial, antifungal, antiviral, antioxidant, anti-inflammatory, hypotensive, antidiabetic, anticonvulsant, and antispasmodic activity [13]. One of these plants' specifications is tangy odor, a nonubiquitous compound due to the attendance of volatile sulfide constituents with significant pharmacological properties [13, 14].

The present study was designed for the biogenic synthesis of AgNPs using *Ferula assafoetida* as reductant/stabilizer (Fer@AgNP) and evaluating its efficacy on four pathogenic bacteria comprising *Staphylococcus aureus*, *Escherichia coli*, *Salmonella typhi*, and *Enterococcus faecalis* compared to aqueous extraction of *Ferula assafoetida* (FerEX) and chemically synthesized AgNP (cAgNP). Also, the biocompatibility of Fer@AgNP was examined thoroughly using human cell lines as well as human red blood cells (RBCs).

2. Materials and Methods

2.1. Aqueous Extraction of Ferula assafoetida (FerEX). *Ferula assafoetida* parts were dehydrated at 18-24°C for 14 days after complete rinsing with deionized water. Afterward, in a glass beaker containing 500 mL of deionized water, 41 g of *Ferula assafoetida* powder was added and boiled at 50°C for 16 h. After cooling, the aqueous extract was filtered using Whatman No. 1 filter paper. Then, until further studies and biological experiments, the black-brown bottle comprising FerEX was kept at 4°C.

Infrared Fourier transform spectroscopy (FT-IR) (Bruker show Tensor II) was applied for its characterization. Also, the compounds found in Ferula assafoetida were analyzed using gas chromatography connected to a mass spectrometer (GC/MS, Agilent Technologies 5975C). The column is of the type HP-5 MS (length 30 m, inner diameter 0.25 mm, and thin layer thickness 0.25 μm). After increasing the oven temperature from 60 to 250°C (thermal gradient of 5°C/min), it was maintained at 250°C for 10 min. Helium gas with ionization energy of 70 electron volts and a flow rate of 1.1 mL/min was used as a carrier. The interface temperature is 280°C. Also, the mass-to-load ratio was in the range of 30-600 m/z. Compounds were identified by injection of C9-C20 hydrocarbons under similar conditions (using retention indices) and comparison with mass spectra suggested by computer libraries according to Willey (nl7) and Adams libraries spectra.

2.2. Synthesis of Biogenic Silver Nanoparticles (Fer@AgNPs). Herein, 5 mL FerEX was poured by sterile pipette into a glass container for the synthesis of Fer@AgNP. A total of 1 mM of silver nitrate ($AgNO_3$, 95 mL) was added and permitted to constant shaking for 48 h at 25°C in a dark chamber (Scheme 1). It could be confirmed that Ag^+ had been reduced to Ag^0, when the color of the solution changed from colorless to brown. The colored solution was centrifuged for 20 min at 4°C at 12,000 rpm and washed three times by centrifugation. Using a vacuum evaporator, the mass was dried, and Fer@AgNP powders were set at 4°C in a degas holder.

2.3. Chemical Synthesis of Silver Nanoparticles. Chemical synthesis of silver nanoparticles (cAgNPs), according to Abbaszadegan et al., was performed by reduction of $AgNO_3$ by $NaBH_4$. In summary, 1 mL of $AgNO_3$ (0.1 mM), previously cooled using ice and stirring, was slowly added to 20 mL of $NaBH_4$ (6.2 mM) [15]. This reaction was kept for 24 hours in a dark room until the next experiment and stored at 4°C.

2.4. Characterizations of Nanomaterials. In this research, cAgNP and Fer@AgNP were characterized through UV-visible spectroscopy, FT-IR spectrometer (Bruker Tensor II), field emission-scanning electron microscope (FE-SEM, Tescan show Mira III), X-ray powder diffraction (XRD) (Tescan show S Max finder Mira III), and energy-dispersive X-ray spectroscopy (EDX, Tescan show S Max locator Mira III).

2.5. Antibacterial Activity. The antimicrobial effect of tested compounds was evaluated using the microdilution broth method and culturing on an agar plate to achieve minimum bactericidal concentrations. The microorganism used in this study includes *Enterococcus faecalis* (ATCC 25922), *E. coli* (ATCC 11700), *Staphylococcus aureus* ATCC 25923, and *Salmonella typhimurium* (ATCC 13311).

2.5.1. Minimum Inhibitory Concentration (MIC). The guidelines provided by the Clinical and Laboratory Standards Institute (CLSI) were used to evaluate the antibacterial susceptibility of the FerEX, cAgNP, and Fer@AgNP. Also, a microdilution broth assay was used to determine the minimum inhibitory concentrations (MICs). Briefly, 100 μL of each compound (in serial concentration from 1000 μg/mL to 7.8 μg/mL with a descending concentration) was added to a 96-well microplate containing 90 μL Mueller-Hinton Broth (MHB), and 10 μL of each microorganism (with the turbidity of 0.5 McFarland) was then transferred to wells under gentle pipetting for homogenizing the mixture. The microplates were incubated at 37°C for 24 h under convenient air and gentle shaking, and then, each well's optical density (OD) was read using an ELIZA reader (BioTek, Winooski, VT, USA). The MIC was obtained based on the following equation:

$$V\% = \frac{A_t - A_b}{A_c - A_b} * 100. \quad (1)$$

V% represents the microorganism viability percent, A_t is the tested well absorbance value, A_c represents the positive control well absorbance value, and A_b is the negative control well absorbance value.

This study used a mixture of MHB and each microorganism as positive control and MHB media as negative control. Each experiment was performed in triplicate.

2.5.2. Minimum Bactericidal Concentration (MBC). Bacterial strains were cultured in MHB media in a different concentration of tested compounds (FerEX, Fer@AgNP, cAgNP) and incubated for 24 h at 37°C to achieve MBC values. Then, 10 μL media from each container were cultured on plates containing Mueller-Hinton agar (MHA) and incubated overnight at 37°C. The MBC for each compound was considered the lowest concentration, resulting in less than four visible colonies, which had been accomplished in triplicate.

2.6. Biocompatibility Evaluations

2.6.1. In Vitro Cellular Cytocompatibility. The MTT standard colorimetric method was used to evaluate the cellular cytocompatibility of tested compounds on the L-929 cell line. Mouse connective tissue fibroblast cell IBRC C10102 (L-929) cells were obtained from the Iranian Biological Research Center and were maintained in the minimum essential medium in Earle's BSS with 1 mM sodium pyruvate and 2 mM L-glutamine supplemented with 10% fetal bovine serum (FBS). A certain number of cells (10^4) was suspended in Dulbecco's modified Eagle medium (DMEM) containing 10% FBS and approximately 1% penicillin and streptomycin and incubated in a humid atmosphere, 5% CO_2, and 95% air at 37°C to achieve cell adherence and reach the confluency about 75-90%. Then, the media were changed by DMEM containing six different concentrations of compounds from 1 to 500 µg/mL and incubated in a humid atmosphere, 5% CO_2, and 95% air at 37°C again for 48 h. Then, the cells were washed with PBS for three minutes, and MTT solution (4 mg/mL [3-(4,5-dimethylthiazol-2-yl)-2,5-diphenyltetrazolium bromide] in DMEM) was added to each cell-containing well, and incubate again for 4 hours. After removing the MTT solution, dimethyl sulfoxide (DMSO) was added and incubated for 10 minutes. The plate was shaken in two orbital manners for 5 min to dissolve the formazan crystals completely. The enzyme-linked immunosorbent assay (ELISA) reader at 540 nm was used to measure the solution's optical absorption (OD). The percent of viable cells was calculated using the following equation:

$$\%\text{cell viability} = \frac{[\text{OD (cell + compound)} - \text{OD (compound)}]}{[\text{OD (cell)} - \text{OD (DMEM)}]} * 100. \quad (2)$$

In this study, wells containing untreated L-929 cells were used for the positive control (100% survival), and wells containing culture medium were used for negative control (0%). This experiment was performed in triplicate.

2.6.2. Hemocompatibility Assay. The hemocompatibility assay was performed to further evaluate the cytocompatibility of Fer@AgNP compared to cAgNPs and FerEX. Accordingly, human red blood cells (hRBCs) were obtained by separating serum through centrifugation of human whole blood at 500g for 10 min. The pellet cells were washed with PBS solution for 3 min at 3000g. Then, 500 μL suspended hRBC was incubated with 200 μg of each tested substance to reach 100 μg/mL concentration. These samples were incubated and shaken at 37°C for 3 h. Finally, the mixtures were centrifuged at 800 rpm for 15 min, the optical absorption of each sample supernatant was read at 570 nm, and the percentage of hemolysis was calculated according to the following equation:

$$\%\text{Hemolysis} = \frac{[\text{OD (hRBC + compound + PBS)} - \text{OD (compound + PBS)}]}{[\text{OD (hRBC + PBS)} - \text{OD (PBS)}]} * 100. \quad (3)$$

Table 1: The most chemical compounds found in *Ferula assafoetida*.

Peak	RT	Height	%	Cal KI	Compound	Reference KI
1	6.005	41997	0.010	913	(Z)-1-Methyl-2-(prop-1-en-1-yl)disulfane	914
2	6.280	712353	0.064	924	Thujene (α-)	930
3	6.502	192273600	25.66	933	Pinene (α-)	939
4	6.747	1632151	0.16	942	Sulfide, butyl propenyl	940
5	6.816	2717964	0.36	945	Camphene	946
6	7.520	140742771	16.31	972	Pinene (β-)	979
7	7.742	8892702	1.4	981	Myrcene	988
8	8.178	1726926	0.22	998	Thiophene, 2,3,4-trimethyl	1002
9	8.637	741709	0.082	1012	Cymene (o-)	1022
10	8.943	4386404	0.53	1021	Limonene	1029
11	9.065	40138134	4.45	1024	Ocimene (Z-β)	1032
12	9.425	20221093	2.38	1035	Ocimene (E-β)	1044
13	12.256	1687896	0.23	1116	Ocimene (allo-)	1132
14	12.700	1165389	0.20	1128	Ocimene (neo-allo-)	1140
15	13.350	2576434	0.44	1145	n-Propyl sec-butyl disulfide	
16	13.572	114265043	23.64	1151	(Z)-sec-Butyl propenyl disulfide	1149
17	13.725	116920126	21.28	1155	(E)-sec-Butyl propenyl disulfide	1163
18	15.347	3052877	0.42	1198	Disulfide, bis(1-methylpropyl)	1212
19	16.762	24485	0.01	1234	(Z)-1-(But-1-en-1-yl)-2-(sec-butyl)disulfane	1255
20	18.537	500196	0.06	1278	Sabinyl acetate (trans-)	1290
21	18.660	490877	0.11	1281	2-Methoxy-4-vinylphenol	1293
22	23.403	3413075	0.71	1299	2-Methyl-5-(1-methylethyl)-phenol	1298
23	23.694	550244	0.14	1403	1-(1-(Methylthio)propyl)-2-propyldisulfane	1405
24	24.689	786685	0.14	1433	Prenyl limonene (cis-)	1443
25	24.804	1413224	0.19	1436	Myltayl-4 (12)-ene	1445
26	25.156	1107851	0.24	1445	Humulene (α-)	1454
27	26.341	465991	0.08	1475	Dihydro agarofuran (4-epi-cis)	1499
28	26.839	2458002	0.37	1488	Dihydro agarofuran (β-)	1503
29	26.999	452015	0.07	1492	Dihydro agarofuran (cis-)	1520
30	27.673	563497	0.08	1510	Cadinene (δ-)	1523
31	30.228	326428	0.05	1579	Carotol	1594
32	30.993	1757758	0.29	1599	Eudesmol (10-epi-γ)	1623

In this study, 100 μL PBS was added to 700 μL PBS as blank, and 100 μL Triton-X-100 (Sigma-Aldrich, USA) in 700 μL PBS was considered positive control. The experiment was performed in triplicate.

2.7. Statistical Analysis. SPSS software version 22.0 (SPSS Inc., Chicago, IL, USA) was used to analyze the biological effects statistically. One-way analysis of variances (ANOVA) followed by Tukey tests was applied to detect the statistical difference between groups in the antibacterial and biocompatibility tests. The number of replicates in this experiment was three times, and 0.05 was considered the degree of significance (significant limit: $p \leq 0.05$).

3. Result and Discussion

3.1. FerEX Constituents. Table 1 shows the most chemical compounds found in *Ferula assafoetida* using GC/MS apparatus. The analysis led to the identification of different mono- and sesquiterpenes as well as volatile sulfur-containing compounds. *Ferula assafoetida* contain 32 different chemical compounds including myrcene (1.4%), butyl disulfides (45.36%), α-pinene (25.66%), β-pinene (16.31%), 2-methyl-5-(1-methylethyl)-phenol (carvacrol) (0.71%), myrcene (1.4%), Z-β-, E-β-, allo-, and neo-allo-ocimene (7.26%), and limonene (0.51%). Recent studies on the analysis of the compounds in the *Ferula assafoetida* had shown results similar to this study but with different amounts and percentages [16, 17]. Although the most abundant compounds found in *Ferula assafoetida* are oxygenated sesquiterpenes, their tang odor was dominated by volatile sulfur-containing constituents. These compounds are important chemotaxonomic markers of Apiaceae [17]. The sec-butyl derivatives of the sulfur-containing compound have previously been reported from *Ferula assafoetida* [18]. Traditionally, this plant is used as an anthelminthic disinfectant for

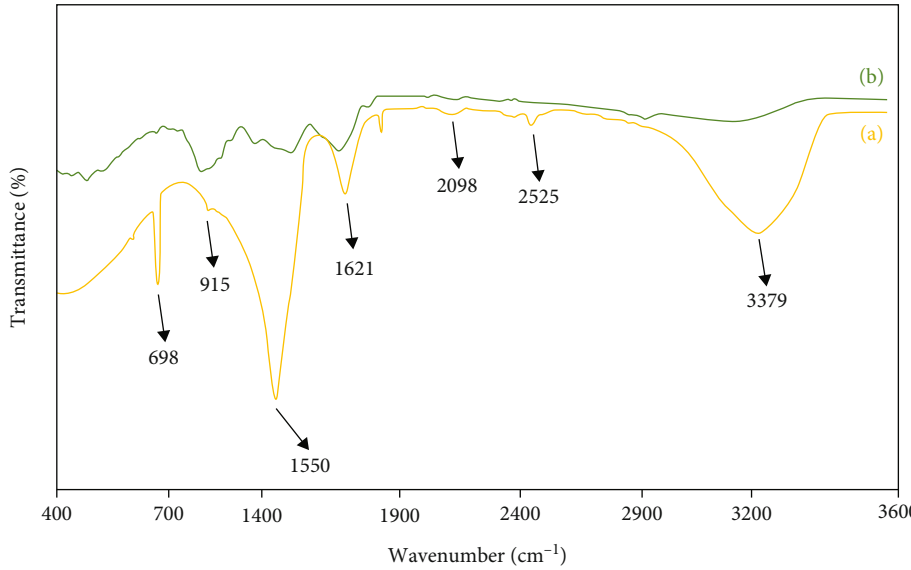

Figure 1: FT-IR spectra of (a) FerEX and (b) Fer@AgNP.

digestive diseases. However, there is no significant information about the biological activities of sulfur components of *Ferula assafoetida*. Two decades ago, Kyung and Lee reported antimicrobial activities of sulfur compounds derived from two plant extracts against various microorganisms, including Gram-positive and Gram-negative bacteria and fungi [19]. They claimed that the principal antimicrobial effect of plants is those belonging to their sulfur components.

3.2. Characterization of AgNPs. After the biogenic synthesis of silver nanoparticles, FT-IR analysis was used to confirm functional groups on the surface of nanoparticles and identify the possible biomolecules responsible for the reduction, capping, and efficient stabilization of silver nanoparticles. Figure 1 shows the FT-IR diagram of FerEX and Fer@AgNP.

The FTIR spectrum of FerEX shows peak positions at 875, 1503, 1612, 2088, and 3301 cm^{-1}, and the FTIR spectrum of Fer@AgNP shows different peak positions at 698, 915, 1550, 1621, 2098, 2525, and 3379 cm^{-1}. There are small marginal shifts in the peak position of Fer@AgNP, indicating the presence of the residual FerEX as a capping agent of Fer@AgNP. The intense broad band at 3379 cm^{-1} may correspond to OH stretching vibrations of polyphenols/carboxylic groups. The weak peak at 25225 cm^{-1} represents thiol (SH) stretching vibration, and a peak at 2098 cm^{-1} is assigned to the alkyne group in phytoconstituents of extract. The peak at 1621 is assigned to carbonyl (C=O) stretching of polyphenols or amide (O=C–N) bending. The powerful band at 1550 cm^{-1} may be assigned to C=C aromatic stretching, and the peaks at 915 and 698 are assigned to C–H alkenes stretch and thioether (C-S) groups, respectively. The peaks in Figures 1(a) and 1(b) appear to be mainly due to secondary metabolites of the FerEX, including triterpenes, resins, flavonoids, tannins, and saponins (Table 1). Previous studies have also proposed such an idea for other plant extracts [20–22]. Colloidal suspensions may result from the interaction of natural functional groups, especially sulfur-containing compounds with silver ions [23]. The mechanism of interaction of metallic silver nanoparticles in a biogenic way is relatively easy from the chemical physics point of view because there were plenty of sulfur-containing compounds and conjugated double bonds in the FerEX solution, as demonstrated by FTIR analysis and GC/MS. These compounds' interactions as reducing and capping agents and silver ions are now well known [7]. In the laboratory, we saw the formation of well-dispersed colloidal suspension within the bowl, which, in turn, verified the formation of AgNPs in the effect of interaction between silver ions and probably sulfur-containing compounds.

Besides, in Figure 2, Fe-SEM pictures of FerEX, cAgNP, and Fer@AgNP have been illustrated. Both the synthesized green and chemical nanoparticles have a circular geometry. As evident in Figures 2(a) and 2(b), biogenic synthesized nanoparticles have a better appearance than chemically synthesized ones, and their colloidal stability is higher. They are quite uniform, with an average size of around 10 ± 2.77 nm. The size and size distribution of chemically synthesized AgNP are 23.5 ± 14.3 nm. Analysis of EDAX mapping showed the main element found in Fer@AgNP (Figure 3).

The X-ray diffraction (XRD) spectrometer confirms the crystalline structure of the synthesized AgNPs, as shown in Figure 4. It illustrated the structure of cAgNP and Fer@AgNP that Ag is confronting face-centered cubic. The X-ray graph uncovered silver nanoparticles; a few diffraction peaks at 2θ of almost 29.4, 32.4, 39.1, and 48.3° correspond to the (111), (200), (220), and (311) Miller indices, respectively. The arrangement of these peaks is due to the natural combinations displayed within the plant extract and dependable for Ag particle lessening and obsession of synthesized Fer@AgNP [24, 25]. These nanomaterials were compared with AgNP utilizing different plant extracts, detailed by other analysts that displayed a comparative crystalline structure for AgNPs [26, 27]. Using the following

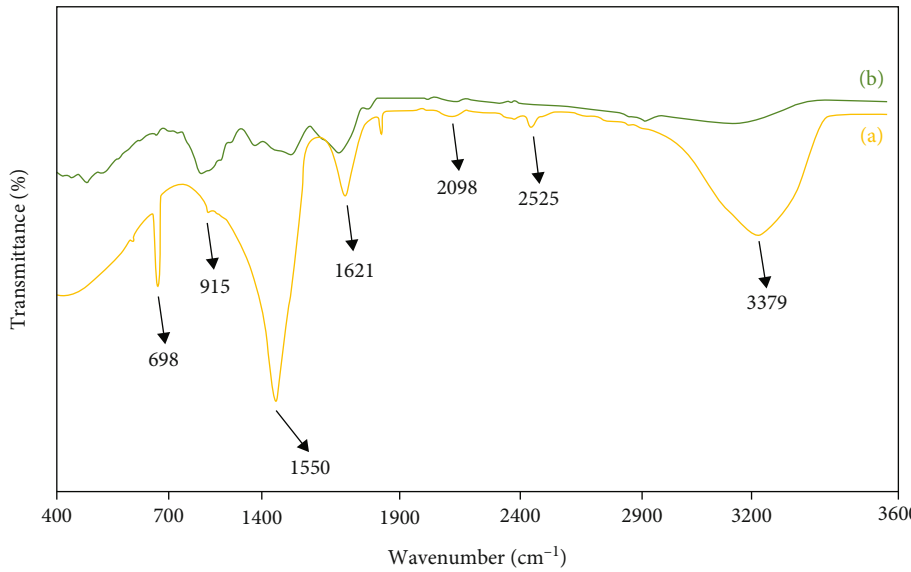

Figure 2: Fe-SEM images of chemically and green synthesized AgNPs: (a) cAgNP and (b) Fer@AgNP.

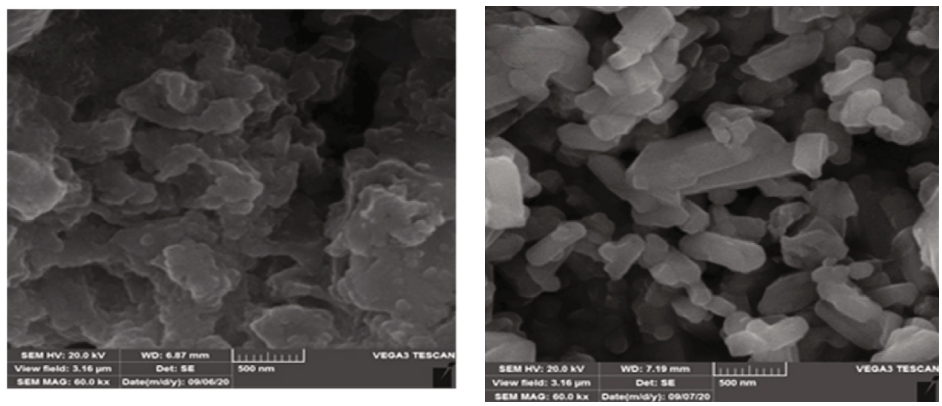

(a) (b)

Figure 3: Analysis of EDAX mapping for green synthesized (Fer@AgNP) nanoparticles.

equation (Debay-Scherer), the average crystalline estimation of silver nanoparticles was measured:

$$D = \frac{K\lambda}{\beta \text{coscos}\,\theta}. \quad (4)$$

In this equation, k could be geometric calculated (0.9), λ is the wavelength of the X-ray radiation source, D is the average crystalline estimate of synthesized NPs, and β is the angular FWHM (full-width at half most extreme) of the XRD top at the diffraction point θ [6, 28]. In this inquiry, using FerEX, the average crystalline sizes were 42.7 and 22.5 nm for cAgNP and Fer@AgNP.

As appears in Figure 5, utilizing UV-visible absorption spectral analysis, the characteristic strong scattering and absorption properties of silver nanoparticles were due to the exposure of the nanoparticles to light at around λ_{max} 450 nm that oscillated electrons of the Ag surface. The gotten range was related to forming silver nanoparticles and agreeing with previous papers. At wavelengths between 400 and 500 nm, the formation range of silver nanoparticles has been described in detail based on the above reports [29, 30]. The peaks in Figure 6 (blue and orange) show that a high-intensity surface plasmon resonance (SPR) band was observed at 426 and 421 nm for the cAgNPs and Fer@AgNP.

3.3. Antibacterial Effects. The antibacterial activity of FerEX, Fer@AgNP, and cAgNP was examined using the microdilution method against both Gram-positive (*S. aureus* and *E. faecalis*) and Gram-negative (*E. coli* and *S. typhi*) bacteria. For the bacterio-inhibition and bactericidal studies according to MIC and MBC, various concentrations of each chemical ranged from 1 to 200 μg/mL. According to the antimicrobial data, the antibacterial properties appeared to increase with compound concentration for all species (Figure 7). The MIC values for cAgNP and Fer@AgNP were 50 to 200 μg/mL and 10 to 50 μg/mL, respectively, compared to 100 and 200 μg/mL for FerEX against all of the bacterial

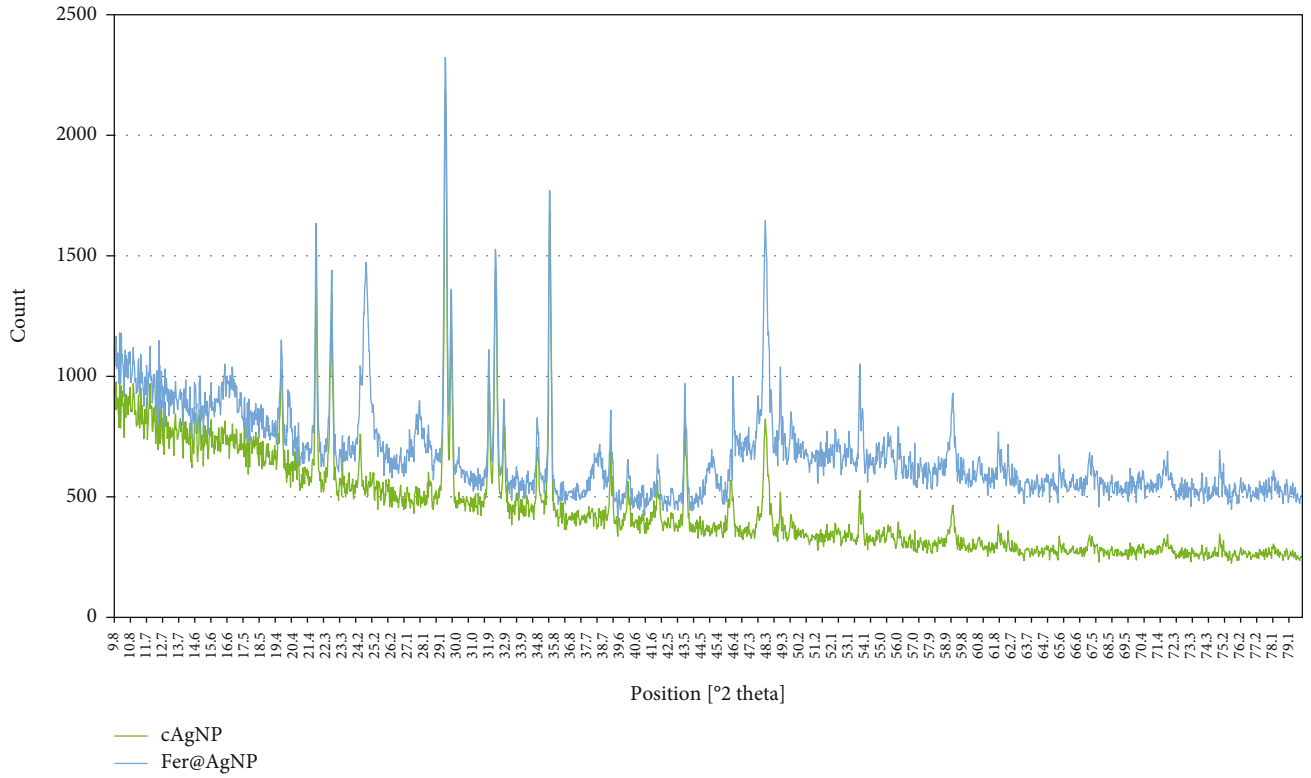

Figure 4: XRD spectra of chemically and green synthesized AgNPs: (orange) cAgNP and (blue) Fer@AgNP for determination of Ag crystals.

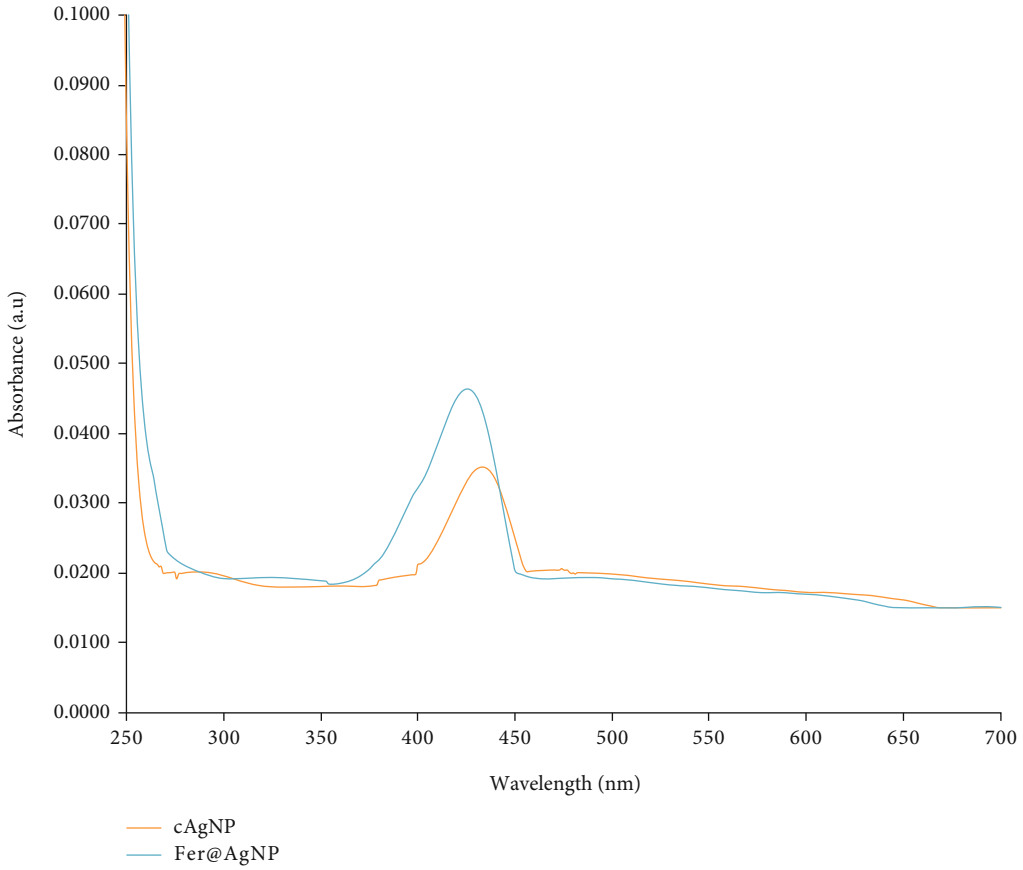

Figure 5: UV-visible spectra of chemically and green synthesized AgNPs: (orange) cAgNP and (blue) Fer@AgNP.

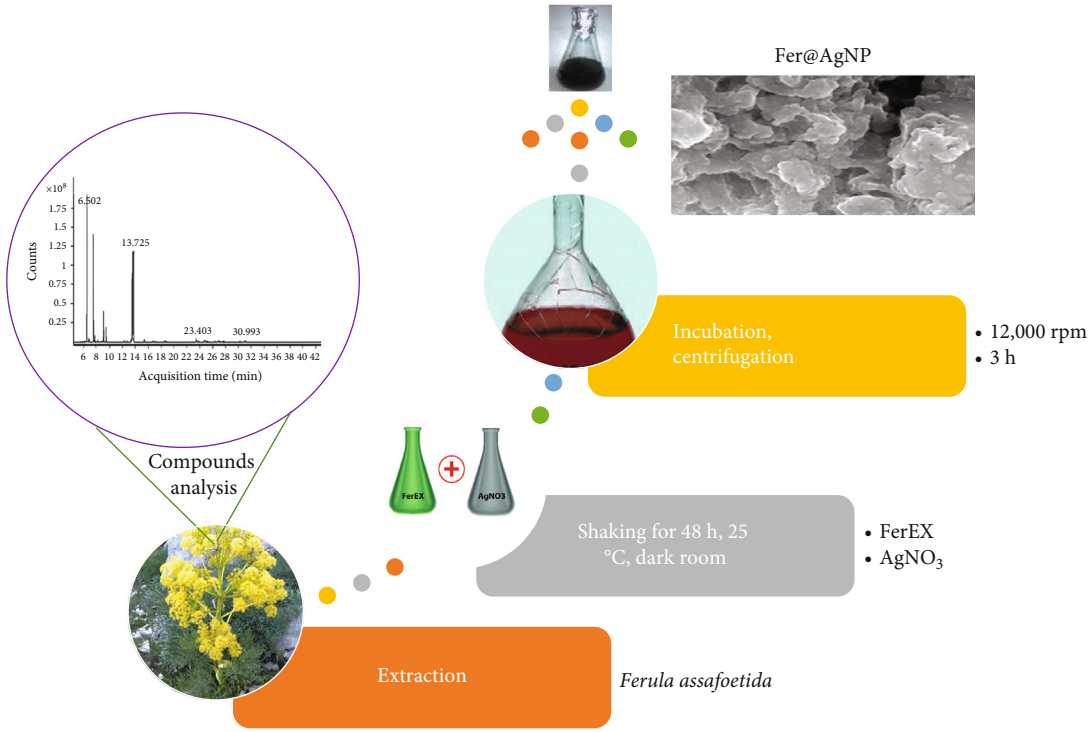

Figure 6: Schematic presentation for the biogenic synthesis of silver nanoparticles (Fer@AgNP) using *Ferula assafoetida* plant extract (FerEX).

strains (Table 2). Compared to Gram-negative bacteria, all of the Fer@AgNPs overall demonstrated better antibacterial tendency against Gram-positive bacteria, as indicated in Table 2. The most potent antibacterial activity against *S. aureus* was displayed by the Fer@AgNPs (Table 2). More specifically, *S. aureus* was the target of Fer@AgNP's most significant antibacterial activity at 10 μg/mL and the same MBC value. However, *E. coli* showed the lowest antibacterial activity of Fer@AgNP, with MIC values of 50 and MBC values of 100 μg/mL. In the study, Fer@AgNP outperformed FerEX and cAgNP in antibacterial and bacterio-inhibition.

Several studies appeared that silver nanoparticles green synthesized by plant extract have a substantial antibacterial effect. These biogenic silver nanoparticles unequivocally restrained the development of a wide range of microbial pathogens, including *Azotobacter chroococcum*, *Bacillus licheniformis*, *Escherichia coli*, *Staphylococcus aureus*, *Candida albicans*, *Pseudomonas aeruginosa*, and *Enterococcus faecalis* related to rather usual hospital-acquired contaminations [28, 31]. In this study, because of their comparatively small size compared to their counterparts (cAgNP), Fer@AgNP exhibits better antibacterial activity against all bacterial strains. The biogenic synthesized nanomaterials probably have a higher surface area than chemically synthesized nanoparticles due to their smaller size. The higher surface area of the nanoparticles, which is connected to their smaller size, allows for better contact with the microbes [15].

An extract of the *Ferula assafoetida* plant was found to contain a variety of secondary metabolites, including resins, oleins, flavonoids, diterpenes, and sulfur-containing tannins, as well as lengthy hydrocarbon chains and other hydrophilic moieties. The interaction of phytoconstituents with the Fer@AgNP was also seen in FTIR spectra. The Fer@AgNPs' negative surface potential may be evidence that their interactions with bacteria were primarily noncovalent (i.e., hydrophobic) [32]. The molecular crowding phenomenon might also be crucial in the interaction between the Fer@AgNP and bacteria. When bacteria are exposed to Fer@AgNP, the interaction between the silver cations released from the nanoparticles and the bacterial cell wall increases the permeability of the cell membrane [33, 34].

A buildup of encapsulated protein precursors and the subsequent denaturation of proteins caused by silver nanoparticles or ions linked to the cell wall made it possible for the nanoparticles to pass through the cell membrane. Silver ions can engage with proteins' thiol groups to render them inactive after entering the cell, or they can interact with DNA to stop DNA replication. In other words, after the encounter, AgNPs gather on the bacterial cell wall, develop pits, and eventually pierce through the cell membrane. The leading cause of bacterial protein denaturation, which results in cell death, is caused by Ag^+ ions from AgNPs [35]. Our data indicate that the antibacterial activity of the Fer@AgNP was superior against Gram-positive bacteria compared to Gram-negative bacteria. This results from the variations in their cell wall composition and structure. Gram-positive and Gram-negative bacteria's different cell membrane compositions provide different absorption channels for nanoparticles. A selective penetration barrier for molecules is formed by the lipopolysaccharides (LPS), lipoproteins, and phospholipids of the cell membrane of Gram-negative bacteria. LPS, which gives the cell membrane a negative charge, is

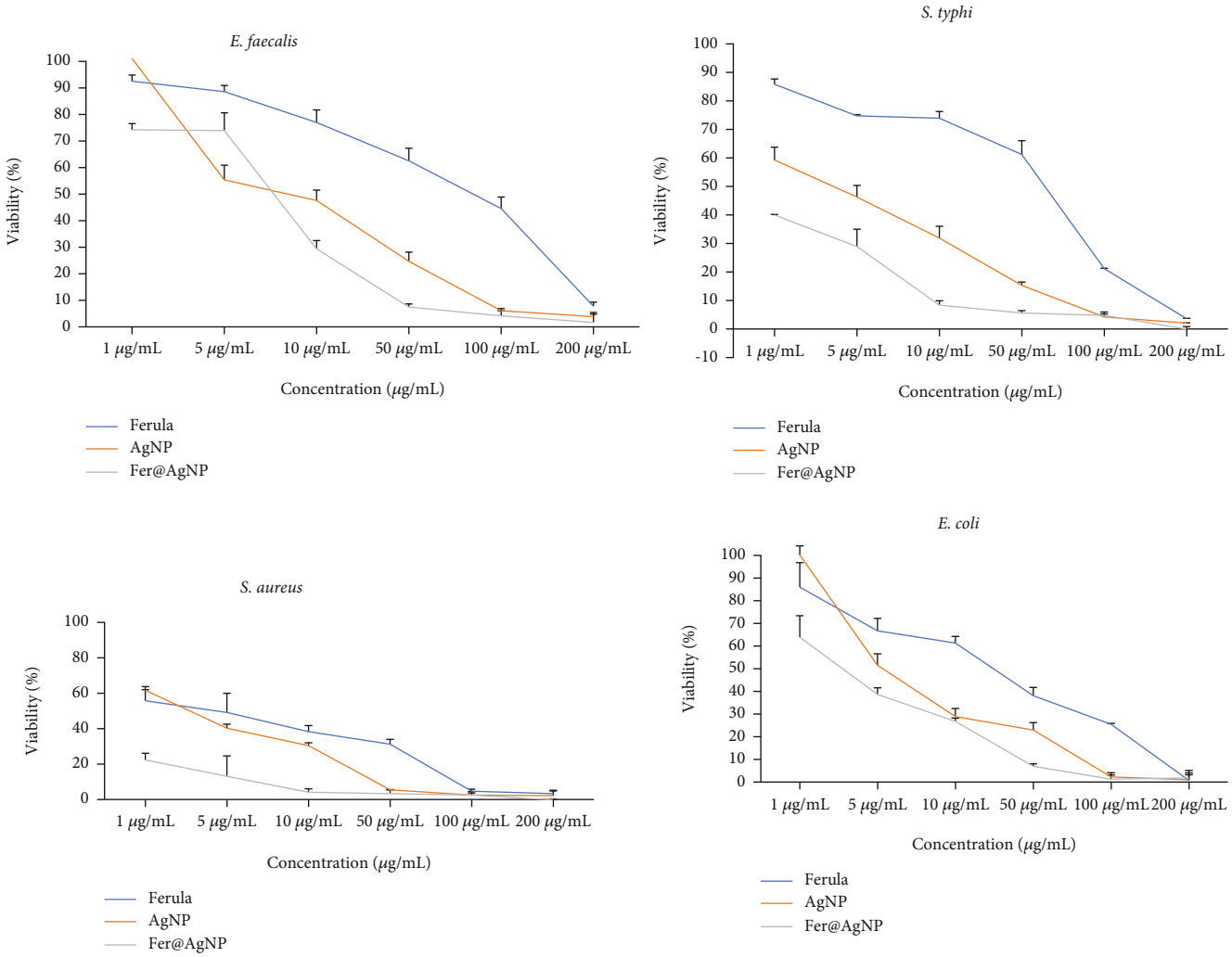

Figure 7: Antimicrobial effects of different concentrations of tested compounds against four pathogenic bacteria using the microdilution method.

Table 2: Quantitative MBC results of biosynthesized AgNP nanoparticles.

Compounds	Microorganisms							
	S. aureus		*E. faecalis*		*E. coli*		*S. typhi*	
	MIC	MBC	MIC	MBC	MIC	MBC	MIC	MBC
FerEX	100 μg/mL	ND*	200 μg/mL	ND	200 μg/mL	ND	200 μg/mL	ND
cAgNP	50 μg/mL	100 μg/mL	100 μg/mL	100 μg/mL	200 μg/mL	100 μg/mL	100 μg/mL	100 μg/mL
Fer@AgNP	10 μg/mL	10 μg/mL	50 μg/mL	50 μg/mL	50 μg/mL	100 μg/mL	10 μg/mL	100 μg/mL

*ND indicates no detection of antimicrobial effect at tested concentrations.

only found in Gram-negative bacteria. Teichoic acid, on the other hand, is only found in the cell walls of Gram-positive bacteria [36].

Additionally, it has numerous pores and a thick layer of peptidoglycan that allow foreign molecules to enter and harm or destroy the cell membrane, ultimately leading to cellular death. Gram-positive bacteria have a higher surface negative charge on their cell walls than Gram-negative bacteria. As a result, the as-produced Fer@AgNP interface more hydrophobically with Gram-positive bacteria and exhibit stronger bactericidal activity [37]. Different antibacterial activities of Fer@AgNP against distinct bacterial strains are caused by variations in lipid membrane chain orientation, membrane gross composition, or unique protein complexes found on the bacterial cell wall surface. This finding is in line with a prior study that found that

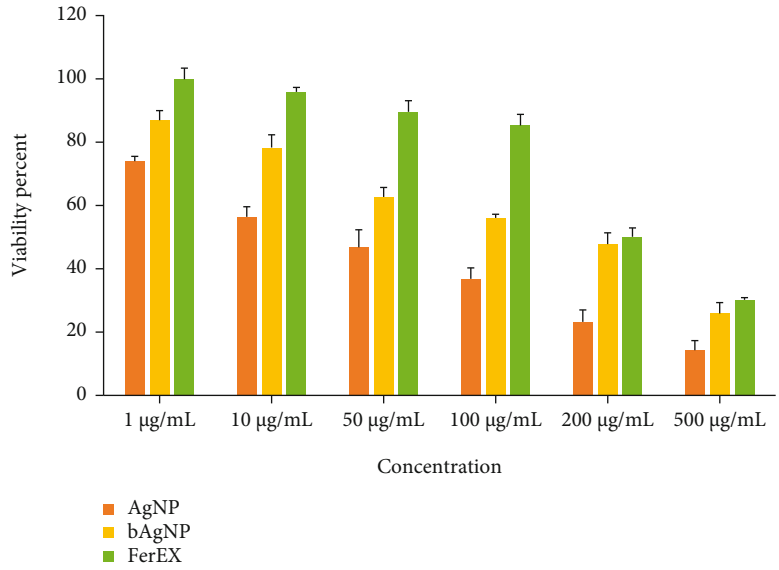

Figure 8: Biocompatibility evaluation of the FerEX, Fer@AgNP, and cAgNP on the L-929 cells for 48 h by MTT assay.

their antibacterial capability also gets stronger as nanoparticles get smaller [32].

Additionally, sulfur-containing compounds on the surface of biogenic synthesized nanoparticles may be responsible for Fer@AgNP's antibacterial action. The typical response between sulfur-containing groups and the -SH groups of vital cellular proteins has been proposed to explain the antimicrobial impact of sulfur-containing compounds. S(O)S groups responsible for the antibacterial activity quickly react with cysteine to produce mixed disulfides [19]. Allicin and thiamine essentially had the same effect, as demonstrated by Adineh et al. [38]. The general reaction can be used in situations where thiosulfinates are present, and the reaction is thought to constitute the typical mechanism of thiosulfinates' antimicrobial activity [19]. Therefore, this significant difference between Fer@AgNP and cAgNP may be related to not only size but also the surface natural compounds, especially sulfur-containing functional groups.

3.4. Biocompatibility Evaluations. The biocompatibility of FerEX, Fer@AgNP, and cAgNP was assessed by quantifying the numbers of viable cells and assessing the percentage of metabolically active cells (L-929 cell line) via the MTT assay revealing that cAgNP at a concentration of 50 μg/mL or higher concentrations was toxic to cells (IC50 = 50 μg/mL, $p < 0.0001$) by day 48 compared to untreated control cells (Figure 8). At 500 μg/mL of Fer@AgNP, some cells survived at a low density (IC50 was not detected, $p < 0.0001$) compared to control. Interestingly, at a concentration of 200 μg/mL or lower, no cytotoxicity was observed compared to untreated controls. The effective antimicrobial concentration of Fer@AgNP (50 μg/mL and 100 μg/mL) showed no significant toxicity compared to the untreated control over 2 days ($p < 0.05$).

The lack of any unfavorable cytotoxic effects from nanoparticles is crucial for any prospective medical application, yet AgNPs have been proven to be toxic not only to bacteria and fungi but also to various animal species and cultured cells [39]. A drawback of previous research evaluating the cytotoxicity of nanomaterials was that the effects of AgNPs could only be seen when the quantities of the two substances approached each substance's respective MIC. However, Abootalebi et al. showed that Fer@AgNP could have potent antibacterial effects at very low concentrations, although they only tested one bacterial strain [8]. Furthermore, although only tested for 24 hours, they found no discernible cytotoxicity towards the hepatocarcinoma cell line (HepG2).

In the current investigation, we expanded on these findings to demonstrate that the normal connective tissue fibroblast (L-929) was still viable after 48 hours of direct culture with Fer@AgNP at low AgNP concentrations, i.e., 1 μg/mL. The literature is still unclear about the precise concentration at which AgNPs may be cytotoxic, largely because of the variety of different production methods and in vitro testing methods that have been employed [40, 41]. Krajewski et al. demonstrated that AgNPs did not cause any hematologic changes at the biocompatible concentration used in this study, whereas 3 μg/mL significantly increased CD11b expression on granulocytes and 30 μg/mL caused hemolysis of erythrocytes, granule secretion in platelets, and activation of the coagulation and complement cascades [42].

3.5. Hemocompatibility Assay. The hemocompatibility of biogenic Fer@AgNPs was compared to AgNP and FerEX using hRBCs for 3 h incubation at 37°C. The hemolytic percent of samples was assessed as a function of the mass concentration of nanoparticles in the real blood mixture at an effective antimicrobial concentration (100 μg/mL), and the results are shown in Figure 9. Among the three samples, chemically synthesized AgNP caused significantly more significant hemolysis ($p < 0.05$), 27% hemolysis. In contrast, FerEX caused less than 13% hemolysis, and Fer@AgNPs showed a very low hemolytic potential (>5%) against

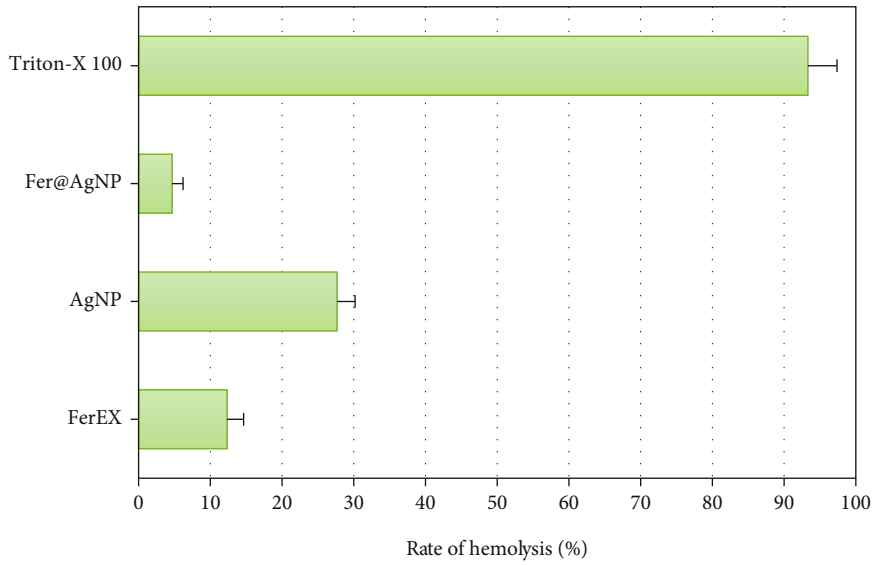

Figure 9: Hemolysis effect of tested compounds against human red blood cells. Hemolysis levels for Fer@AgNP were significantly different from the positive control (Triton-X) and AgNP at $p < 0.05$; however, the statistical significance is not shown in the figure.

hRBCs. According to the ASTM E2524-08 standard, substances that cause hemolysis by more than 5% can potentially damage RBCs [43]; therefore, chemically synthesized AgNP at a concentration of 100 μg/mL is potentially hemotoxic, while biogenic AgNP, which indicates excellent hemocompatibility, can be considered biocompatible. The results of Triton X-100 as positive control verified the performance of the hemocompatibility assay.

The hemolytic activity of chemically synthesized AgNPs may be due to pore formation in the membrane of erythrocytes, changing membrane integrity, and surface characteristics of nanoparticles and osmotic lysis [44]. Natural capping agents such as FerEX with many biogenic polymers protected the cell membrane from hemolytic shock through a mechanism involving colloid-osmotic lysis of the erythrocytes [45]. This in vitro osmotic protection may not happen in the circulating bloodstream due to insufficient polymer concentrations. Also, the release of Ag^+ from AgNPs could induce lipid peroxidation (LPO) and RBC hemolysis, probably due to reactive oxygen species (ROS) generation. Ag^+ seems to interact with mitochondrial inner membrane thiol groups and is inferred in the proper function of mitochondria.

The excellent cytocompatibility of Fer@AgNP is supposed to be because of various natural compounds, including peptides, phenolic compounds, and polysaccharides found in FerEX at the surface of AgNPs. These compounds appear to slow the release of Ag^+ from nanoparticles, and as a result, the antioxidant mechanisms of the cell have ample opportunity to eliminate these toxic ROS and reduce their toxicity. Also, the zeta potential of Fer@AgNP may play a role, which results in the electrostatic repulsion between the AgNPs and charged RBC membrane. These proposed mechanisms need to confirm in the future detailed mechanism study.

It was demonstrated that the biocompatible concentration of AgNPs utilized in this investigation improved microbial death. Interestingly, antibiotics that target both Gram-positive and Gram-negative bacteria showed synergistic benefits, pointing to a nonspecific multimodal mechanism of action. According to Saratale et al., nanoparticles can attach to the bacterial cell membrane, creating pits on the cell surface that allow penetration into the cell where AgNPs have a greater affinity to react with biomolecules like DNA that contain sulfur or phosphorous, preventing DNA replication and causing cell death [46]. Similarly, AgNPs may interact with thiol groups found in enzymes like NADH dehydrogenase to assault and disrupt the respiratory chain specifically. AgNPs' general attenuation of the bacteria as a result of their nonspecific antibacterial activity aids in preventing the emergence of bacterial resistance.

4. Conclusion

Conclusively, this study demonstrated the rationality of the green synthesis of *AgNPs* utilizing an aqueous extract of FerEX. Due to the attendance of groups comprising thiol and groups of alkyl halide and other reducing agents within the extricate of FerEX, reducing silver particles to nanoparticles occurs. This green Fer@AgNP revealed a high antibacterial movement on four pathogenic bacteria. It is interesting to note that at high concentrations, the synthesized green nanoparticles could not initiate a noteworthy diminish in cell practicality of L-929 cells. Future experiments may examine the long-term and other perspectives of antimicrobial such as biofilm restraint and substantivity, as well as the different potential advantageous effects on irresistible illnesses.

Data Availability

All data used to support the findings of this study are included within the article.

Conflicts of Interest

The authors declare that they have no conflicts of interest.

Funding

This study was conducted based on license no. 22484 after obtaining the grant.

Acknowledgments

The study was funded by the Vice-Chancellor for Research, Shiraz University of Medical Sciences, Shiraz, Iran. The authors thank Mr. H. Argasi for his invaluable assistance in the Research Consulting Center of Shiraz University of Medical Sciences in editing this manuscript.

References

[1] S. M. Mousavi, G. Behbudi, A. Gholami et al., "Shape-controlled synthesis of zinc nanostructures mediating macromolecules for biomedical applications," *Biomaterials Research*, vol. 26, no. 1, pp. 1–20, 2022.

[2] A. Gholami, F. Mohammadi, Y. Ghasemi, N. Omidifar, and A. Ebrahiminezhad, "Antibacterial activity of SPIONs versus ferrous and ferric ions under aerobic and anaerobic conditions: a preliminary mechanism study," *IET Nanobiotechnology*, vol. 14, no. 2, pp. 155–160, 2020.

[3] T. A. Abalkhil, S. A. Alharbi, S. H. Salmen, and M. Wainwright, "Bactericidal activity of biosynthesized silver nanoparticles against human pathogenic bacteria," *Biotechnology & Biotechnological Equipment*, vol. 31, no. 2, pp. 411–417, 2017.

[4] A. Gholami, K. Ghezelbash, B. Asheghi, A. Abbaszadegan, and A. Amini, "An in vitro study on the antibacterial effects of chlorhexidine-loaded positively charged silver nanoparticles on Enterococcus faecalis," *Journal of Nanomaterials*, vol. 2022, Article ID 6405772, 8 pages, 2022.

[5] J. Mittal, A. Batra, A. Singh, and M. M. Sharma, "Phytofabrication of nanoparticles through plant as nanofactories," *Advances in Natural Sciences: Nanoscience and Nanotechnology*, vol. 5, no. 4, article 043002, 2014.

[6] S. Zargarnezhad, A. Gholami, M. Khoshneviszadeh, S. N. Abootalebi, and Y. Ghasemi, "Antimicrobial activity of isoniazid in conjugation with surface-modified magnetic nanoparticles against Mycobacterium tuberculosis and nonmycobacterial microorganisms," *Journal of Nanomaterials*, vol. 2020, Article ID 7372531, 9 pages, 2020.

[7] A. Gholami, M. S. Shams, A. Abbaszadegan, and M. Nabavizadeh, "Ionic liquids as capping agents of silver nanoparticles. Part II: antimicrobial and cytotoxic study," *Green Processing and Synthesis*, vol. 10, no. 1, pp. 585–593, 2021.

[8] S. N. Abootalebi, S. M. Mousavi, S. A. Hashemi, E. Shorafa, N. Omidifar, and A. Gholami, "Antibacterial effects of green-synthesized silver nanoparticles using Ferula asafoetida against Acinetobacter baumannii isolated from the hospital environment and assessment of their cytotoxicity on the human cell lines," *Journal of Nanomaterials*, vol. 2021, Article ID 6676555, 12 pages, 2021.

[9] A. Abbaszadegan, S. Dadolahi, A. Gholami et al., "Antimicrobial and cytotoxic activity of Cinnamomum zeylanicum, calcium hydroxide, and triple antibiotic paste as root canal dressing materials," *The Journal of Contemporary Dental Practice*, vol. 17, no. 2, pp. 105–113, 2016.

[10] A. Abbaszadegan, S. Sahebi, A. Gholami et al., "Time-dependent antibacterial effects of Aloe vera and Zataria multiflora plant essential oils compared to calcium hydroxide in teeth infected with Enterococcus faecalis," *Journal of Investigative and Clinical Dentistry*, vol. 7, no. 1, pp. 93–101, 2016.

[11] A. Abbaszadegan, A. Gholami, Y. Ghahramani et al., "Antimicrobial and cytotoxic activity of Cuminum cyminum as an intracanal medicament compared to chlorhexidine gel," *Iranian Endodontic Journal*, vol. 11, no. 1, pp. 44–50, 2016.

[12] P. Mahendra and S. Bisht, "Ferula asafoetida: traditional uses and pharmacological activity," *Pharmacognosy Reviews*, vol. 6, no. 12, pp. 141–146, 2012.

[13] A. Amalraj and S. Gopi, "Biological activities and medicinal properties of Asafoetida: a review," *Journal of Traditional and Complementary Medicine*, vol. 7, no. 3, pp. 347–359, 2017.

[14] S. M. Mousavi, S. A. Hashemi, H. Esmaeili, A. M. Amani, and F. Mojoudi, "Synthesis of Fe_3O_4 nanoparticles modified by oak shell for treatment of wastewater containing Ni (II)," *Acta Chimica Slovenica*, vol. 65, no. 3, pp. 750–756, 2018.

[15] A. Abbaszadegan, M. Nabavizadeh, A. Gholami et al., "Positively charged imidazolium-based ionic liquid-protected silver nanoparticles: a promising disinfectant in root canal treatment," *International Endodontic Journal*, vol. 48, no. 8, pp. 790–800, 2015.

[16] V. Karimian, P. Ramak, and J. T. Majnabadi, "Chemical composition and biological effects of three different types (tear, paste, and mass) of bitter *Ferula assa-foetida* Linn. gum," *Natural Product Research*, vol. 35, no. 18, pp. 3136–3141, 2021.

[17] J. Kasaian, J. Asili, and M. Iranshahi, "Sulphur-containing compounds in the essential oil of Ferula alliacea roots and their mass spectral fragmentation patterns," *Pharmaceutical Biology*, vol. 54, no. 10, pp. 2264–2268, 2016.

[18] M. Iranshahy and M. Iranshahi, "Traditional uses, phytochemistry and pharmacology of asafoetida (*Ferula assa-foetida* oleo-gum-resin) –a review," *Journal of Ethnopharmacology*, vol. 134, no. 1, pp. 1–10, 2011.

[19] K. Kyung and Y. Lee, "Antimicrobial activities of sulfur compounds derived from S-Alk (en) yl-L-cysteine sulfoxides in Alliumand Brassica," *Food Reviews International*, vol. 17, no. 2, pp. 183–198, 2001.

[20] K. Dhivya, "Screening of phytoconstituents, UV-VIS spectrum and FTIR analysis of *Micrococca mercurialis* (L.) Benth," *International Journal of Herbal Medicine*, vol. 5, no. 6, pp. 40–44, 2017.

[21] S. Ramya, T. Loganathan, M. Chandran et al., "Phytochemical screening, GCMS, FTIR profile of bioactive natural products in the methanolic extracts of Cuminum cyminum seeds and oil," *Journal of Drug Delivery and Therapeutics*, vol. 12, no. 2-S, pp. 110–118, 2022.

[22] N. Omidifar, A. Nili-Ahmadabadi, A. Gholami, D. Dastan, D. Ahmadimoghaddam, and H. Nili-Ahmadabadi, "Biochemical and histological evidence on the protective effects of Allium hirtifolium boiss (Persian Shallot) as an herbal supplement in cadmium-induced hepatotoxicity," *Evidence-based complementary and alternative medicine*, vol. 2020, Article ID 7457504, 8 pages, 2020.

[23] K. Afshinnia, B. Marrone, and M. Baalousha, "Potential impact of natural organic ligands on the colloidal stability of

silver nanoparticles," *Science of the Total Environment*, vol. 625, pp. 1518–1526, 2018.

[24] S. Pirtarighat, M. Ghannadnia, and S. Baghshahi, "Green synthesis of silver nanoparticles using the plant extract of Salvia spinosa grown in vitro and their antibacterial activity assessment," *Journal of Nanostructure in Chemistry*, vol. 9, no. 1, pp. 1–9, 2019.

[25] S. A. Hashemi, S. M. Mousavi, and S. Ramakrishna, "Effective removal of mercury, arsenic and lead from aqueous media using polyaniline-Fe_3O_4- silver diethyldithiocarbamate nanostructures," *Journal of Cleaner Production*, vol. 239, article 118023, 2019.

[26] M. Ghaffari-Moghaddam, R. Hadi-Dabanlou, M. Khajeh, M. Rakhshanipour, and K. Shameli, "Green synthesis of silver nanoparticles using plant extracts," *Korean Journal of Chemical Engineering*, vol. 31, no. 4, pp. 548–557, 2014.

[27] A. U. Khan, Q. Yuan, Z. U. H. Khan et al., "An eco-benign synthesis of AgNPs using aqueous extract of *Longan* fruit peel: antiproliferative response against human breast cancer cell line MCF-7, antioxidant and photocatalytic deprivation of methylene blue," *Journal of Photochemistry and Photobiology B: Biology*, vol. 183, pp. 367–373, 2018.

[28] O. E. Rodríguez-Luis, R. Hernandez-Delgadillo, R. I. Sánchez-Nájera et al., "Green synthesis of silver nanoparticles and their bactericidal and antimycotic activities against oral microbes," *Journal of Nanomaterials*, vol. 2016, Article ID 9204573, 10 pages, 2016.

[29] M. Ndikau, N. M. Noah, D. M. Andala, and E. Masika, "Green synthesis and characterization of silver nanoparticles using Citrullus lanatus fruit rind extract," *International Journal of Analytical Chemistry*, vol. 2017, Article ID 8108504, 9 pages, 2017.

[30] S. M. Mousavi, S. A. Hashemi, M. Zarei et al., "Recent progress in chemical composition, production, and pharmaceutical effects of kombucha beverage: a complementary and alternative medicine," *Evidence-based Complementary and Alternative Medicine*, vol. 2020, Article ID 4397543, 14 pages, 2020.

[31] R. Singh, J. Vora, S. B. Nadhe, S. A. Wadhwani, U. U. Shedbalkar, and B. A. Chopade, "Antibacterial activities of bacteriagenic silver nanoparticles against nosocomialAcinetobacter baumannii," *Journal of Nanoscience and Nanotechnology*, vol. 18, no. 6, pp. 3806–3815, 2018.

[32] M. M. Hossain, S. A. Polash, M. Takikawa et al., "Investigation of the antibacterial activity and in vivo cytotoxicity of biogenic silver nanoparticles as potent therapeutics," *Frontiers in Bioengineering and Biotechnology*, vol. 7, p. 239, 2019.

[33] S. Priyadarshini, V. Gopinath, N. Meera Priyadharsshini, D. MubarakAli, and P. Velusamy, "Synthesis of anisotropic silver nanoparticles using novel strain, *Bacillus flexus* and its biomedical application," *Colloids and Surfaces B: Biointerfaces*, vol. 102, pp. 232–237, 2013.

[34] F. Mohammadi, A. Gholami, N. Omidifar, A. Amini, S. Kianpour, and S. M. Taghizadeh, "The potential of surface nano-engineering in characteristics of cobalt-based nanoparticles and biointerface interaction with prokaryotic and human cells," *Colloids and Surfaces B: Biointerfaces*, vol. 215, article 112485, 2022.

[35] K. S. Siddiqi, A. Husen, and R. A. Rao, "A review on biosynthesis of silver nanoparticles and their biocidal properties," *Journal of Nanobiotechnology*, vol. 16, no. 1, pp. 1–28, 2018.

[36] M. S. Niloy, M. M. Hossain, M. Takikawa et al., "Synthesis of biogenic silver nanoparticles usingCaesalpinia digynaand investigation of their antimicrobial activity andin vivobiocompatibility," *ACS Applied Bio Materials*, vol. 3, no. 11, pp. 7722–7733, 2020.

[37] L. Wang, C. Hu, and L. Shao, "The antimicrobial activity of nanoparticles: present situation and prospects for the future," *International Journal of Nanomedicine*, vol. 12, pp. 1227–1249, 2017.

[38] H. Adineh, M. Harsij, H. Jafaryan, and M. Asadi, "The effects of microencapsulated garlic (*Allium sativum*) extract on growth performance, body composition, immune response and antioxidant status of rainbow trout (*Oncorhynchus mykiss*) juveniles," *Journal of Applied Animal Research*, vol. 48, no. 1, pp. 372–378, 2020.

[39] D. S. Ipe, P. T. S. Kumar, R. M. Love, and S. M. Hamlet, "Silver nanoparticles at biocompatible dosage synergistically increases bacterial susceptibility to antibiotics," *Frontiers in Microbiology*, vol. 11, 2020.

[40] T. Shi, X. Sun, and Q.-Y. He, "Cytotoxicity of silver nanoparticles against bacteria and tumor cells," *Current Protein and Peptide Science*, vol. 19, no. 6, pp. 525–536, 2018.

[41] J. R. Nakkala, R. Mata, and S. R. Sadras, "Green synthesized nano silver: synthesis, physicochemical profiling, antibacterial, anticancer activities and biological *in vivo* toxicity," *Journal of Colloid and Interface Science*, vol. 499, pp. 33–45, 2017.

[42] S. Krajewski, R. Prucek, A. Panacek et al., "Hemocompatibility evaluation of different silver nanoparticle concentrations employing a modified Chandler-loop in vitro assay on human blood," *Acta Biomaterialia*, vol. 9, no. 7, pp. 7460–7468, 2013.

[43] J. Choi, V. Reipa, V. M. Hitchins, P. L. Goering, and R. A. Malinauskas, "Physicochemical characterization and in vitro hemolysis evaluation of silver nanoparticles," *Toxicological Sciences*, vol. 123, no. 1, pp. 133–143, 2011.

[44] H. Huang, W. Lai, M. Cui et al., "An evaluation of blood compatibility of silver nanoparticles," *Scientific Reports*, vol. 6, no. 1, pp. 1–15, 2016.

[45] T. Kwon, H. J. Woo, Y. H. Kim et al., "Optimizing hemocompatibility of surfactant-coated silver nanoparticles in human erythrocytes," *Journal of Nanoscience and Nanotechnology*, vol. 12, no. 8, pp. 6168–6175, 2012.

[46] G. D. Saratale, R. G. Saratale, G. Benelli et al., "Anti-diabetic potential of silver nanoparticles synthesized with Argyreia nervosa leaf extract high synergistic antibacterial activity with standard antibiotics against foodborne bacteria," *Journal of Cluster Science*, vol. 28, no. 3, pp. 1709–1727, 2017.